Residual compressive stress prediction determined by blade edge radius and feed rate during milling of thin-walled parts

Xiaohui Jiang
Yan Cai
Weiqiang Liu
Miaoxian Guo (miaoxian.guo@live.com)
University of Shanghai for Science and Technology https://orcid.org/0000-0001-8411-7051
Hong Zhou
Zhou Xu
Xiangjing Kong
Pengfei Ju

Research Article

Keywords: Thin-walled parts, Prediction model, Simulation, Active control

Posted Date: June 3rd, 2022

DOI: https://doi.org/10.21203/rs.3.rs-1657665/v1

Abstract

Residual compressive stress can effectively improve fatigue life of aerospace thin-walled parts. In this study, residual compressive stress control is taken as the target. Firstly, a surface residual stress prediction model is proposed, which considers both machining parameters and milling force-heat. The model of the relationship between milling force, thermal load and residual stress is established, which quantifies the effects of mechanical and thermal loads on the formation of residual compressive stresses. The results show that the feed rate of each tooth and the blade edge radius play an important role in the residual compressive stress of the milling surface. The prediction models of surface residual stress for thermal load, mechanical load, feed per tooth and radius are established. Secondly, the ratio α of the feed rate per tooth f_z to the blade edge radius r is calculated. When $\alpha_{xx} = 0.42 \sim 0.65$ and $\alpha_{yy} = 0.36 \sim 0.7$, the surface residual compressive stress in X and Y directions of the workpiece reaches the maximum value. Thus, the ratio of the feed rate per tooth f_z to the blade edge radius r is optimized to control the mechanical and thermal load quantization. It realizes active control of residual compressive stress on workpiece surface.

1. Introduction

In order to meet the high speed, reliable and lightweight development requirements of high-performance components in aerospace, thin-walled parts are the preferred products. Aluminum alloy has the advantages of light weight, high strength and corrosion resistance. It is often used as a machining material for large thin-walled parts in the aerospace field [1]. It is easy to produce residual stress and deformation of aluminum alloy thin-walled parts in milling due to the influence of cutting load, clamping force, vibration of machine tool spindle and other factors. This greatly reduces the workpiece machining accuracy. Existing research shows that reducing the residual stress on the surface of parts or changing the tensile stress into compressive stress in the actual machining process. This method can effectively improve the comprehensive performance of parts [2]. Therefore, it is important to find a method to predict and control the generation of residual compressive stress during machining.

In view of the distribution of residual stress during machining, many scholars have studied it from the perspective of process parameters and tool parameters. As for the process parameters, Chighizola et al. [3] carried out the milling experiment on Al7050 aluminum plate and measured the surface residual stress. It was found that the depth of surface residual stress increased with the increase of feed per tooth and was not affected by the cutting speed. Wu et al. [4] conducted simulation analysis and experimental verification of residual stress on milling surface of Ti-10V-2Fe-3Al, and established the formula for the relationship between residual stress and feed speed, cutting speed and depth of cut. Rahul et al. [5] studied the effects of critical uncut chip thickness, blade radius, feed per tooth and axial depth on residual stress through finite element model. The results show that cutting force and residual stress increase with increasing blade radius. Woste et al. [6] studied the influence of process parameters on residual stress depth and found that the increase of cutting thickness led to greater compressive stress value and layer number. Jiang et al. [7] found that the residual impact stress generated by the combination of low speed, large feed rate and large cutting depth was much smaller than that generated by the combination of other process parameters at the cutting position and cutting position of the tool. This method could effectively reduce the residual impact stress. Ji et al. [8] conducted an experimental study on the residual stress distribution in the milling process of 2219 aluminum alloy. The results show that the axial cutting depth is the most important factor affecting the residual stress distribution on the machining surface. However, it is not difficult to find that most of the existing researches focus on the analysis of the process parameters affecting the formation of residual stress, and less on the analysis of the main process combination of the formation of residual compressive stress.

In addition, the relationship between the tool parameters and the residual stress was also studied by simulation and experiment. Clauss et al. [9] studied the effects of different clearances and rake angles on milling surface performance and found that the absolute value of compressive residual stress was the highest when the tool was used with a positive rake angle of 5°, which increased by about 290% compared with the initial state. Borysenko et al. [10] studied the influence of tool rake angle on the normal residual stress of the workpiece by combining finite element simulation with actual test. Holmberg et al. [11] used new and worn ceramic and carbide tools to milling 718 inconel grooves. The study showed that tool wear changed the distribution of stress on the grooves and the depth of stress affected. Liang et al. [12] proposed a multi-physical model to predict the residual stress distribution of Ti-6Al-4V orthogonal turning by considering the geometric changes of the tool. The experimental results show that the surface residual stress changes from compressive stress to tensile stress with the change of tool wear degree, and the depth of residual stress moving into the workpiece increases with the increase of tool wear. Liu et al. [13] simulated the influence of tool geometry on the residual stress by using the coupled Euler-Lagrange method, and found that the tool with negative rake angle and sharp edge radius would generate more residual compressive stress on the machined surface. It can be seen that the existing researches have made a good breakthrough in residual stress generation by changing tool parameters alone, but there is still a lack of comprehensive control of residual compressive stress combined with process parameters.

According to the research results of the above scholars, the experimental method has laid a good foundation for mastering the distribution law of machining residual stress. In order to better realize the prediction of residual stress, many scholars put forward the prediction model of residual stress based on the study of the influence of machining parameters on residual stress. Yi et al. [14] established the calculation model of residual stress and milling parameters for side milling and end milling, and the prediction error of the model was 0-14MPa. Cheng et al. [15] studied the surface residual stress under different cutting parameters and machining characteristics, proposed a machining residual stress prediction method based on Gaussian process regression, and found that the feed per tooth had the greatest influence on the surface residual stress relative to the cutting speed and cutting depth. Zhou et al. [16] proposed an analytical model to predict residual stress in complex surface milling under different cutting conditions, and analyzed the influence of tool lead/inclination angle, feed speed and spindle speed on residual stress. Wolfle et al. [17] proposed a numerical scheme for predicting milling induced residual stress, providing sufficient efficiency for real-time applications; Yue et al. [18] established a prediction model of milling force and machine surface residual stress based on the analysis of orthogonal cutting geometric relationship, providing a theoretical basis for stress control. Therefore, various residual stress prediction methods have been proposed, but there is still a lack of prediction models that take residual compressive stress as the control target and take process and tool parameters into consideration.

At present, there are many results to study the influence of single process parameters and tool parameters on the residual stress of workpiece. However, there are few studies on the prediction and control of residual compressive stress based on the combination of mechanical-thermal coupling and machining parameters. Existing studies have shown that the blade edge radius and the feed per tooth are closely related to the generation of milling forces and residual compressive stress in the machining process [19]. On this basis, the relationship between the blade edge radius and the feed per tooth and the milling force and heat is further explored. A residual stress prediction model for machining parameters and thermo-mechanical coupling was established. Moreover, the quantization method of the feed per tooth and the blade edge radius is used to realize the active control of the residual compressive stress on the workpiece surface.

2. Methodology

This part mainly consists of the establishment of residual stress prediction model, experimental setting and simulation process setting. In section 2.1, the mechanical-thermal coupling relationship of residual stress generation is analyzed and the prediction model of residual stress is established. Section 2.2 introduces the material parameters of the experimental workpiece, as well as the experimental equipment and measurement methods for measuring milling force, milling temperature and residual stress. Section 2.3 Simulation model establishment.

2.1 Establishment of prediction model of surface residual stress

2.1.1 Relation between surface residual stress and thermal-mechanical load

Mechanical load and thermal load are important reasons for the formation of residual stress. Machining parameters play an important role in the formation of residual stress. Figure 1 shows the formation mechanism of residual stress in orthogonal cutting [20]. The main cutting speed is much greater than the feed speed in this study.Qualitative descriptions of orthogonal milling models are used to generate cutting force and stress zones.As shown in the figure, x direction is the main cutting direction, y direction is the feed direction, and z direction is the axial direction. F_x, F_y and F_z are the sum of the cutting force components along three directions. The resultant force in each direction is affected by various factors including the feed per tooth and the radius of the blade edge. The material near the processing area 1 in the figure is subjected to extrusion and friction by the blunt round part of the cutting edge and the back cutter face.Plastic deformation and springback occur during milling.This friction force will introduce tensile plastic strain on the material surface.The tensile elastic strain is introduced into the workpiece.The internal release of tensile elastic strain will introduce residual compressive stress, which is attributed to the joint effect of F_x and F_y. When milling, it produces cutting heat.The surface of the workpiece shrinks as it cools.Therefore, the thermal effect will form the residual tensile stress on the surface.Zone 2 is the shear deformation zone.It is mainly caused by the shear force between the tip and the chip, which is attributed to the effect of F_x and the introduction of residual compressive stress in the surface layer.Zone 3 is the area of compression deformation formed by the extrusion of chip and uncut area.

2.1.2 Analysis of milling forces

In the milling process, the stress state of the workpiece is shown in Fig. 3. As shown in Fig. 3(a), at any position angle β, the tangential force dF_t, radial force dF_r and axial force dF_a of the K-th cutting edge element can be expressed as Eq. (1) [21]:

$$\begin{cases} dF_t = K_m \cdot t_c \cdot dz \\ dF_r = K_n \cdot t_c \cdot dz \\ dF_a = K_a \cdot t_c \cdot dz \end{cases}$$

1

Among them, K_m, K_n and K_a are tangential, radial and axial milling force coefficients respectively, t_c is the instantaneous undeformed chip thickness, and d_z is the beveled cutting element.

The transformation of Eq. (1) into Cartesian coordinate system can be written as follows:

$$\begin{cases} dF_x = -dF_t \cdot \cos\beta - dF_r \cdot \sin\beta \\ dF_y = dF_r \cdot \sin\beta - dF_t \cdot \cos\beta \\ dF_z = -dF_a \end{cases}$$

2

By integrating along the axis of the cutting edge, the total cutting force in the X-Y-Z direction is expressed as follows [22]:

$$\begin{cases} F_x = \sum_{k=1}^{k} \int_{U_0}^{U_1} \left[k_m t_c \cos\beta + k_n t_c \sin\beta \right] dz \\ F_y = \sum_{k=1}^{k} \int_{U_0}^{U_1} \left[k_n t_c \cos\beta + k_m t_c \sin\beta \right] dz \\ F_z = \sum_{k=1}^{k} \int_{U_0}^{U_1} -k_a t_c dz \end{cases}$$

3

Where, F_x, F_y and F_z are the total tangential force, radial force and axial force of the cutting edge respectively; U_0 and U_1 are the upper and lower limits of the integral, and K is the number of cutting edges.

The 3D milling model was transformed into a 2D orthogonal cutting model, as shown in Fig. 3(b). In the cutting process, the total force refers to the sum of the forces acting on the tool side and cutting edge as well as on the tool surface, and is the sum of the radial force and axial force of Eq. (2). The force directly acting on the blade edge is called plough force F_p, which is caused by the elastic and plastic deformation of the workpiece material around the blade edge [23]. The force generated by the contact between the chip and the tool surface is the chip forming force F_{ch}. In the cutting process as shown in Fig. (b), the total cutting force F_c in the cutting direction of the milling cutter is composed of the component force $F_{ch,x}$ of the chip forming force in the cutting direction and the component force F_{px} of the plow cutting force in the cutting direction. The total cutting force F_f perpendicular to the cutting direction is composed of the component force $F_{ch,x}$ of chip forming force perpendicular to the cutting direction and the component force F_{py} of plough cutting force perpendicular to the cutting direction.

$$\begin{cases} F_c = -F_r = F_{ch,x} + F_{px} \\ F_f = -F_t = F_{ch,y} + F_{py} \end{cases} \quad (4)$$

As shown in Fig. 3, the workpiece milling force is related to the blade geometry and the feed per tooth. In this work, the machining force, heat and residual stress data of different feed rate per tooth and blade edge radius are studied, and the residual stress prediction model is built according to the data analysis results.

2.1.3 Prediction model of surface residual stress

Mechanical load can form residual tensile stress or compressive stress according to the direction of force, while thermal load will form residual tensile stress. Therefore, the residual stress after mechanical-thermal coupling action needs comprehensive analysis, and is mainly dominated by cutting force [24]. In this study, a prediction model of residual stress on side milling surface was established, which was related to milling process parameters and mechanical and thermal parameters. According to the analysis in Section 2.1.1, F_x and F_y will make the workpiece surface subjected to tension and extrusion, which mainly affects the generation of the residual compressive stress of the workpiece, while the milling temperature causes the residual tensile stress of the workpiece. The prediction model assumes the form of Eq. (5). In the formula, "+" and "-" indicate the tensile and compressive effects.

$$\sigma = +f(\Delta T) - f_1\left(F_x\right) - f_2\left(F_y\right) \quad (5)$$

Among them, ΔT is the temperature change during milling; F_x and F_y are the milling force in the milling direction and feed direction.

This prediction model mainly considers the effect of mechanical load, and the temperature variation in the prediction model can approximate the temperature condition of the processed surface of the workpiece. F_x and F_y are the resultant forces of each stress component in the X and Y directions during milling. As shown in Fig. 7, the influence of F_z and F_x on the generation of residual stress is almost completely proportional, and F_x represents the influence of horizontal force. As shown in Fig. 2, the force in the x and y directions of the workpiece is equivalent to the two projected planes [25], the horizontal length of the projection plane of F_x is approximately the milling depth a_p. The vertical length is approximated to the sum of the function values of the feed per tooth and the radius of the blade edge radius, suppose the radius of the blade edge is $f_4(r)$. F_x is equivalent to Eq. (6). In this study, a_p is fixed, so F_x is equivalent to Eq. (7). The horizontal length of the projection plane of F_y is approximately the sum of the function of V_c and the radius of the blade arc, and the vertical length is approximately a_p. Assuming that the radius of the edge is $f_5(r)$, F_y is equivalent to Eq. (8), and a_p is a constant value. Therefore, F_y is equivalent to Eq. (9).

$$F_x \Leftrightarrow \frac{F_x}{a_p \times \left(f_z + f_4(r)\right)} \quad (6)$$

$$F_x \Leftrightarrow \frac{F_x}{f_z + f_4(r)} \quad (7)$$

$$F_y \Leftrightarrow \frac{F_y}{a_p \times \left(V_c + f_5(r)\right)} \quad (8)$$

$$F_{\mathrm{y}} \Leftrightarrow \frac{F_y}{f_5(r) + V_c} \quad (9)$$

Since the relationship between force and heat during machining and residual stress on workpiece surface is not clear, they are assumed to be nonlinear functions, and the influence of each parameter on residual stress is expressed by exponential function. The functional relationship between force and heat on residual stress on workpiece surface is shown in Eq. (10)-Eq. (12).

$$f(\Delta T) = A \times \left(T_{\max} - T_{normal}\right)^p = A \times (\Delta T)^p \quad (10)$$

$$f_1\left(F_x\right) = B \times \left(\frac{F_x}{f_z + r^{m1}}\right)^{m2}$$

11

$$f_2\left(F_y\right) = C \times \left(\frac{F_y}{r^{n1} + V_c}\right)^{n2}$$

12

Based on the above, the surface residual stress prediction model as shown in Eq. (13):

$$\sigma = A \times \Delta T^p - B\left(\frac{F_x}{f_z + r^{m1}}\right)^{m2} - C\left(\frac{F_y}{r^{n1} + V_c}\right)^{n2}$$

13

Where, A, B and C are the scaling coefficients determined by the measured data; *m1*, *m2*, *n1*, *n2*, *p* and *q* are exponential coefficients. The units of $\Delta T$is, ,F_x and F_y are in N, f_z and R are in mm, and V_c is in m/min.

2.2 Experiment setup

Aluminum alloy material is widely used in the processing of parts in aerospace and other fields. The material selected in this study is Al7075-T6, which has good corrosion resistance, high strength to weight ratio and high thermal conductivity. The material parameters are listed in Table 1. The thermal, mechanical and physical properties of aluminum alloy are shown in Table 2.

Table 1
The main chemical composition of al7075-T6 alloy [26]

Al	Zn	Mg	Cu	Cr	Fe	Si	Ti	Mn
Bal	5.8	2.3	1.5	0.21	0.16	0.07	0.02	0.05

In the experimental part of this study, the CarverS600B machining center of Beijing Carving Technology Group Co. LTD. was used for side milling of the workpiece whose length, width and height were 60mm*40mm*12mm.Before machining, the stress was removed without considering the influence of initial residual stress. In order to predict and verify the surface residual stress, 16 tests were carried out on the specimen, and the processing parameters were set as shown in Table 3. The experimental parameters for verification of residual stress prediction model and residual compressive stress control method in section 4.3 are shown in Table 6.

Table 2
Thermal-mechanical physical properties of Al7075-T6 alloy [29]

Density ρ/(kg·m^{-3})	Specific heat capacity ψ/(J·kg^{-1}·°C^{-1})	Thermal conductivity *M*/(W/mK)	Poisson's ratio	Yield modulus /GPa	Hardness (HV)	Tensile strength (MPa)
2810	960	41.7	0.33	71.7	175	572

The Kistler dynamometer assembly was used for the milling force test. The force measurement range of the dynamometer X, Y and Z directions was ± 250N. The sensitivity in X and Z directions was − 26PC /N, and the sensitivity in Y direction was − 13PC /N. The number of channels for the amplifier was 8; The sampling frequency of the acquisition system was 200kHz. The workpiece was fixed on the dynamometer through the fixture, and the cutting force signal was amplified by the amplifier, and then the data processing software Dynoware was used to process the data. The K - type thermocouple and temperature acquisition card were used to measure the milling heat. After machining, the workpiece surface residual stress was measured by Proto LXRD X-ray stress analyzer. The target material was Cr, and the parameters such as aperture, test voltage, elastic constant K, Bragg Angle and diffraction plane were 1 mm, 25 keV, 98.6124 MPa/degree, 156.31° and 222.

The machining and measurement process are shown in Fig. 4.

Table 3 Experimental processing parameters

Experimental number	Feed per tooth f_z(mm)	Tool edge radius r(μm)	Cutting speed V_c (m/min)	Other parameters
1	0.025	13	150.8	z = 3; R = 4mm;
2	0.01	13	201.1	a_p=5mm;
3	0.015	13	251.3	a_e=2mm
4	0.02	13	301.6	
5	0.025	15	201.1	
6	0.01	15	150.8	
7	0.015	15	301.6	
8	0.02	15	251.3	
9	0.025	18	251.3	
10	0.01	18	301.6	
11	0.015	18	150.8	
12	0.02	18	201.1	
13	0.025	30	301.6	
14	0.01	30	251.3	
15	0.015	30	201.1	
16	0.02	30	150.8	

2.3 Simulation setup

Finite element simulation technology is the most commonly used method to calculate and predict residual stress. In this paper, AdvantEdge FEM, a special software for metal cutting simulation, is used to simulate the milling process, and the Power Law material constitutive model provided by AdvantEdge material library is selected, as shown in Eq. (14).

$$\sigma\left(\varepsilon^p, \dot{\varepsilon}, T\right) = g\left(\varepsilon^p\right)\Gamma\left(\dot{\varepsilon}\right)\Theta(T)$$

14

Where,$\sigma\left(\varepsilon^p, \dot{\varepsilon}, T\right)$is the flow stress of the workpiece material;$g\left(\varepsilon^p\right)$is the strain strengthening function;$\Gamma\left(\dot{\varepsilon}\right)$is the strain rate effect function;$\Theta(T)$is the thermal softening function. Among them,$\varepsilon^p$is the strain during the material deformation process, $\dot{\varepsilon}$is the strain rate during the material deformation process, is the temperature during the material deformation process.

$g\left(\varepsilon^p\right)$ is given by Eq. (15):

$$g\left(\varepsilon^{p}\right)=\begin{cases}\sigma_{0}\left(1+\dfrac{\varepsilon^{p}}{{\varepsilon_{0}}^{p}}\right)^{1/n}, \varepsilon^{p}<{\varepsilon_{cut}}^{p}\\ \sigma_{0}\left(1+\dfrac{{\varepsilon_{cut}}^{p}}{{\varepsilon_{0}}^{p}}\right)^{1/n}, \varepsilon^{p}\geqslant{\varepsilon_{cut}}^{p}\end{cases}$$

15

Where σ_0 , ε^p , ${\varepsilon_0}^p$ and ${\varepsilon_{cut}}^p$ are initial yield stress, plastic strain, reference plastic deformation, cut-off strain value; *n* is the plastic deformation coefficient.

$\Gamma\left(\dot{\varepsilon}\right)$ is given by Eq. (16):

$$\Gamma\left(\dot{\varepsilon}\right)=\begin{cases}\left(1+\dfrac{\dot{\varepsilon}}{\dot{\varepsilon}_{0}}\right)^{\frac{1}{m_1}}, \dot{\varepsilon}\leqslant\dot{\varepsilon}_{t}\\ \left(1+\dfrac{\dot{\varepsilon}}{\dot{\varepsilon}_{0}}\right)^{\frac{1}{m_2}}\left(1+\dfrac{\dot{\varepsilon}_{t}}{\dot{\varepsilon}_{0}}\right)^{\left(\frac{1}{m_1}-\frac{1}{m_2}\right)}, \dot{\varepsilon}>\dot{\varepsilon}_{t}\end{cases}$$

16

Where $\dot{\varepsilon}$, $\dot{\varepsilon}_0$, and $\dot{\varepsilon}_t$ are strain rate, reference plastic strain rate, critical strain value for transition between high and low strain rate sensitivity coefficients; m_1 and m_2 are the sensitivity coefficients of low and high strain rate.

$\Theta(T)$ is given by Eq. (17):

$$\Theta(T)=\begin{cases}c_0+c_1T+c_2T^2+c_3T^3+c_4T^4+c_5T^5, T<T_{cut}\\ \Theta\left(T_{cut}\right)\left(1-\dfrac{T-T_{cut}}{T_{melt}-T_{cut}}\right), T\geqslant T_{cut}\end{cases}$$

17

Where: C_0 - C_5 are polynomial fitting coefficients; T, T_{cut}, and T_{melt} are temperature, linear cutoff temperature and melting temperature.

In this paper, 2D orthogonal cutting simulations are performed on the milling process of the workpiece. The length and height of the workpiece are 3mm and 6mm. The accuracy of 2D simulation module of the software has been demonstrated in previous studies [28]. At the end of the simulation, the results are shown in Fig.5. The forces and residual stresses in the X and Y directions of the workpiece and the cutting temperature are extracted.

3. Validation Of Simulation Model

In order to verify the accuracy of the simulation, the parameters shown in Table 4 were simulated and experimentally verified. The experimental and simulation methods are shown in Sections 2.2 and 2.3.

Table 4
Experimental and simulation parameters

Group	Feed rate per tooth f_z(mm/tooth)	Tool edge radius r(mm)	Cutting speed V_c (m/min)	Workpiece material	Other parameters
1	0.033	0.013	150.8	Al7075-T6	z = 3; R = 4mm; a_p=5mm; a_e=2mm
2	0.033	0.018	100.5	Al7075-T6	
3	0.1	0.018	100.5	Al7075-T6	

It can be seen from Figure 6 that the experimental results of residual stress in X and Y directions are in good agreement with the simulation results. The error value between simulation and experiment is between 5.3MPa-29MPa, and the error is between 11.9%-21%. The milling surface shows residual compressive stress, and the actual value is lower than the simulation value, because there is a certain release of residual stress between machining and measurement.

4. Results And Discussion

In this section, the relationship between milling force and residual stress on workpiece surface is analyzed by experimental results. The unknown coefficient was determined by fitting the surface residual stress prediction model in Section 2.1. The simulation model in Section 2.3 is used to analyze and quantify the influence of f_z and the value of r on the residual stress of the workpiece. Finally, the prediction model and the quantization method of machining parameters are verified by the application experiment.

4.1 Analysis of the relationship between milling force and milling parameters and residual stress on workpiece surface

The milling force during machining will produce tensile and compressive stresses on the workpiece surface. As shown in Fig.3(b), the chip forming force F_{ch} and ploughing force F_p in the cutting process of the tool can be decomposed into component forces in X and Y directions. The component forces parallel to the workpiece surface mainly form residual tensile stress on the workpiece surface, and the residual compressive stress is formed by component forces perpendicular to the workpiece surface. As shown in Fig.7, when F_x, F_y and F_z increase, the residual compressive stress on workpiece surface increases linearly with the increase of milling force. The effects of F_x and F_z on residual stress generation are almost proportional to each other. The dotted line in Fig.7 is to show the variation trend of residual stress with the force, and does not have any numerical meaning.

As shown in Fig. 3(b), when f_z increases, the chip forming force and the X and Y components of the workpiece surface also increase. On the contrary, when f_z is small enough, less than r, as shown in Fig. 9(a), the instantaneous chip forming force on the workpiece is small enough, and the workpiece is only affected by the ploughing force. In a certain range, when the ratio of f_z to r is smaller, θ is smaller, the component force F_{py} perpendicular to the workpiece surface becomes larger, and the component force F_{px} parallel to the workpiece surface becomes smaller, the resultant force F_c in Eq. (4) becomes smaller and F_f becomes larger. Therefore, the residual tensile stress of mechanical load on the workpiece surface decreases, and the residual compressive stress is easy to form. In the residual stress test results of machining parameters shown in Table 3, under the same conditions, when f_z is less than r, the residual compressive stress value on the workpiece surface is relatively larger. As shown in Fig. 8, the residual compressive stress value in the X direction of experimental group 15 increases by 49.8% compared with experimental group 12, and the residual compressive stress value in the Y direction increases by 5.9%. In order to quantify the influence of the relationship between the feed per tooth and blade edge radius on the residual stress, the finite element analysis simulation analysis was carried out in Section 4.3.

4.2 Calculation and discussion of surface residual stress prediction model

Experimental parameters and measurement results as shown in Table 3 are used in this section. It fits the unknown parameters of the residual stress prediction model established in Section 2.1.4. There are 8 parameters to be fitted. The input parameter is the temperature change. The forces F_x and F_y in the X and Y directions of the workpiece, feed per tooth f_z, radius of the blade arc r, milling speed V_c. Output parameters are residual stress values in X and Y directions. Due to the complex equation form, nonlinear curve fitting is used. The confidence interval was 0.05. The residual stresses in X and Y directions of the workpiece surface were fitted by parameters. The fitting results are as follows:

$$\begin{cases} \sigma_{xx} = -8.21\times10^{4}\times\Delta T^{-2.8113} + 5668.96\times\left(\dfrac{F_x}{f_z + r^{1.44\times10^{4}}}\right)^{-0.00275} - 5.98\times10^{3}\times\left(\dfrac{F_y}{r^{-1.76}+V_c}\right)^{0.01067} \\ \sigma_{yy} = -1.779\times10^{8}\times\Delta T^{-5.7954} - 1.266\times10^{-40}\times\left(\dfrac{F_x}{f_z + r^{-0.06116}}\right)^{25.87798} - 976.8167\times\left(\dfrac{F_y}{r^{-82.503}+V_c}\right)^{0.00874} \end{cases} \quad (18)$$

According to Eq. (18), F_x has little influence on the residual stress in the Y direction. The maximum error between the fitting value and the actual value of surface residual stress in X direction is 15.5% and the minimum error is 0.2%. The maximum error between the fitting value and the actual value of surface residual stress in Y direction is 15.6% and the minimum error is 0.1%. The details are shown in Table 5.

Table 5
Error of predicted value relative to experimental value

Experimental number	Residual stress in X direction σ_{xx}(MPa)			Residual stress in Y direction σ_{yy}(MPa)		
	experimental value	predictive value of Eq. (18)	Relative error/%	experimental value	predictive value of Eq. (18)	Relative error/%
1	-63.4	-73.2	15.5%	-51.9	-46.8	9.8%
2	-86.9	-87.8	1.0%	-39.1	-43.9	12.3%
3	-93.5	-89.5	4.3%	-37.9	-43.8	15.6%
4	-145.5	-145.8	0.2%	-92.5	-92.7	0.2%
5	-147.1	-125.2	14.9%	-45.1	-49.6	10.0%
6	-89.3	-99.1	11.0%	-48.6	-48.4	0.4%
7	-106.6	-94.3	11.5%	-45.8	-48.2	5.2%
8	-88.9	-76.3	14.2%	-53.8	-52.7	2.0%
9	-148.3	-129.6	12.6%	-91.5	-91.4	0.1%
10	-116.5	-119.2	2.3%	-55.0	-54.9	0.2%
11	-133.4	-146.8	10.0%	-54.9	-55.2	0.5%
12	-118.5	-121.6	2.6%	-76.1	-65.1	14.5%
13	-175.3	-158.1	9.8%	-71.7	-79.7	11.1%
14	-175.6	-181.2	3.2%	-82.3	-79.6	3.3%
15	-177.5	-176.5	0.6%	-80.6	-79.6	1.2%
16	-162.8	-161.0	1.1%	-79.0	-79.7	0.9%

In the fitting value of residual stress in the Y direction, the coefficient of F_x correlation function is small. This indicates that the influence of F_y on the residual stress in the Y direction is greater than that of F_x. Therefore, relative to the surface residual stress in X direction, the slope of F_y and surface residual stress in Y direction in Fig. 7(c) is closer to 1. Similarly, in Fig. 7(a), it can be seen that the influence of F_x on the residual stress on the X-direction surface is greater than that on the Y-direction surface. The validation of Eq. (18) is shown in Section 4.4

4.3 Quantitative analysis of the influence of blade edge radius and feed per tooth on residual compressive stress generation

It can be seen from section 4.1 that the radius of the blade arc and the parameters of feed per tooth play a major role in the generation of residual stress. Quantifying the relationship between the two can control the generation of residual compressive stress during machining. In this section, the finite element simulation is used to analyze the relationship between r and f_z and the residual stress. The relationship between machining parameters is quantified to achieve the generation of controlling residual compressive stress on workpiece surface.

4.3.1 Analysis of the influence of blade edge radius on residual stress

In this part, 10 different blade edge radius were set. The 2D orthogonal cutting simulation model in Section 2.1.2 was used to analyze the influence of blade arc radius on residual stress.The milling speed ,depth of cut and feed per tooth were respectively 301.6m/min,5mm and 0.05mm.The simulation results are shown in Fig. 10.

In previous studies, the large residual tensile stress generated during machining will accelerate the deformation of the workpiece and affect its life. The lower residual tensile stress or residual compressive stress will delay the fatigue failure time of the workpiece [2]. As can be seen from Fig. 10(a), if r is 0.02mm-0.08mm, the maximum residual compressive stress in the X direction is 0mm.It is shown that the residual compressive stress produced by r is strongest at the machined surface. If r is 0.1mm-0.5mm, the residual stress curve shows a negative extreme value around 0.25mm. This indicates that the optimal position of residual compressive stress at the arc radius of these blades is near the depth of 0.25mm. The maximum residual compressive stress in the X direction of the workpiece surface is at r= 0.08mm.

The position of residual stress curve in Fig. 10(b) can be judged as follows. In Y direction, the negative extremum of all residual stress curves is located near the depth of 0.3mm. After milling, the residual stress of the surface in Y direction is compressive stress. The maximum value of residual compressive stress in Y direction on the workpiece surface is -229MPa at r= 0.1mm. Combined with the analysis results of residual stress in X direction, the residual compressive stress on the workpiece surface reaches the peak value if r is about 2 times f_z.

4.3.2 Analysis of the influence of feed per tooth on residual stress

In the previous section, the influence of the blade edge radius on the generation of residual compressive stress was analyzed under the condition of constant feed per tooth.It is found that the residual compressive stress on the workpiece surface reaches the peak value when the ratio of r to f_z is about 2.To further quantify this ratio, this section used two cutting tools with different blade edge radius of 0.1mm and 0.2mm.Both tools were set with multiple different f_z.The influence of different f_z on residual stress is analyzed.The simulation results are shown in Fig. 11-Fig. 12.

According to Fig. 11(a), when r= 0.1mm and f_z=0.02mm-0.05mm, the maximum residual compressive stress in the X direction appears at 0mm.This indicates that the best place for residual stress generation is on the machined surface. When the depth from surface is greater than 0.6mm, the difference of residual stress becomes smaller. This indicates that the residual stress is less affected by f_z. It can be seen from Fig. 12(a) that it behaves if r is 0.2mm. The maximum residual compressive stress in X direction is located at the machined surface when f_z=0.06mm-0.15mm.

The residual stress curve in the Y direction in Fig. 11(b) can be seen as follows. When r= 0.1mm and f_z=0.02mm-0.05mm, the maximum residual compressive stress corresponding to f_z is located on the machining surface. According to Fig. 12(b), the specific details are as follows. When r= 0.2mm and f_z=0.02mm-0.1mm, the maximum residual compressive stress is located on the machined surface. The residual stress curve is divided into two parts around f_z=0.05mm when r= 0.1mm. Only when f_z <0.05mm, the maximum residual compressive stress appears on the workpiece surface. Similarly, r= 0.2mm and f_z <0.1mm, the maximum residual compressive stress appears on the workpiece surface.

It can be seen from the above analysis that the residual stress distribution on the workpiece surface changes regularly with the ratio of r and f_z. It assumes that the ratio of f_z and r is shown in Eq. (19):

$$\frac{f_z}{r} = \alpha \tag{19}$$

It is substituted into the surface residual stress prediction formula Eq. (18). The result is shown in Eq. (20). Combined with the analysis results in Fig. 10-Fig. 12, the surface residual stress values in X and Y directions can be obtained. The details are shown in Fig. 13.

$$\sigma_{xx} = -8.21 \times 10^4 \times \Delta T^{-2.8113} + 5668.96 \times \left(\frac{F_x}{\alpha \times r + r^{1.44 \times 10^4}} \right)^{-0.00275} - 5.98 \times 10^3 \times \left(\frac{F_y}{r^{-1.76} + V_c} \right)^{0.01067}$$

$$\sigma_{yy} = -1.779 \times 10^8 \times \Delta T^{-5.7954} - 1.266 \times 10^{-40} \times \left(\frac{F_x}{\alpha \times r + r^{-0.06116}} \right)^{25.87798} - 976.8167 \times \left(\frac{F_y}{r^{-82.503} + V_c} \right)^{0.00874}$$

20

According to the variation trend in Fig. 13(a), when r= 0.1mm, f_z=0.05mm ~ 0.06mm, that is a_{xx} = 0.5 ~ 0.6, the residual compressive stress in the X direction is the maximum. When f_z=0.06mm ~ 0.07mm, that is a_{yy} = 0.6 ~ 0.7, the residual compressive stress in the Y direction is the maximum. Similarly, r= 0.2mm, the residual compressive stress in the X and Y directions takes the maximum value respectively when a_{xx} = 0.55 ~ 0.65 and a_{yy} = 0.6 ~ 0.65. According to Fig. 13(b), when f_z=0.05mm and a_{xx} = 0.42 ~ 0.63, the residual compressive stress in the X direction of the workpiece surface is the maximum. In the same way, a_{yy} = 0.36 ~ 0.5, the residual compressive stress in the Y direction of the workpiece surface is the maximum. In conclusion, when a_{xx} = 0.42 ~ 0.65, the surface residual compressive stress in the X direction of the workpiece reaches the maximum. When a_{yy} = 0.36 ~ 0.7, the surface residual compressive stress in Y direction is the maximum.

4.4 Verification of the prediction model of surface residual stress and method of quantification of milling parameters

In order to verify the accuracy of the quantitative relationship between the residual stress and the prediction model of f_z and r, 6 groups of aluminum alloy parts with the size of $50mm \times 50mm \times 40mm$ were processed separately in this section. The material was the same as the workpiece used in Table 3. First, the inner cavity was roughed with three edge flat-bottomed cutter ϕ8mm, spindle speed 8000 rpm, cutting depth 3 mm, feed rate 0.1mm/tooth. Then, the workpiece was processed into a thin-walled frame part with a wall thickness of 4mm with ϕ3mm flat end milling cutter, spindle speed 12000 rpm, cutting depth 0.25 mm, feed rate 0.4mm/tooth. The machining parameters shown in Table 6 were used to process the parts along the external surface into a thin-walled part with a wall thickness of 2mm after the stress removal treatment. It was processed by filling the inner cavity with paraffin to reduce the deformation when milling the outer surface. The residual stress on the outer surface of 6 groups of parts was measured respectively. Six points were randomly selected on the outer test surface to test the residual stress value, and the average value was taken as the residual stress value. Milling experimental instruments and specific test procedures are shown in Section 2.2.

The details are as shown in Fig. 14. Under the condition that r and V_c are constant, the milling temperature and the milling force in each direction of the thin-walled part increase linearly with the increase of f_z. According to the experimental results, when V_c and r were constant, the force and temperature of group A are smaller than that of group B and C. The working part of group A is f_z =0.5r. The milling forces F_x and F_y are 44.6% and 21.8% smaller than those of group C with f_z >0.5r. Similarly, the milling force in X and Y direction of group E is 30.1% and 9.1% smaller than that of group F.

Table 6
Experimental machining parameters

Group	A	B	C	D	E	F
Feed per tooth f_z(mm)	0.01	0.025	0.03	0.01	0.015	0.02
Tool edge radius r(mm)	0.02	0.02	0.02	0.03	0.03	0.03
Cutting speed V_c (m/min)	201.1	201.1	201.1	201.1	201.1	201.1
Other parameters	z = 3; R = 4mm; a_p=5mm; a_e=2mm					

In order to verify the proposed surface residual stress prediction model, the milling parameters in Table 6 and the measured milling force and temperature change parameters were substituted into Eq. (13). The predicted and actual measured values of surface residual stress were shown in Fig. 15.The error between the predicted value and the actual test value of the surface residual stress in the X direction is

between 10.6% and 17.5% and that in the Y direction is 8.7%-18.8%. As can be seen from the experimental results in Fig. 15, other processing conditions were the same, the residual compressive stress in X and Y directions of the working parts in group E is the maximum. a_{xx} and a_{yy} of group E are both 0.5, the residual compressive stress in X and Y directions are respectively 16.2% and 18.1% higher than that in group F. α_{xx} and α_{yy} of group A are both 0.5. The residual compressive stress in X direction is 9.5% higher than that in group B. The residual compressive stress in the Y direction increased by 16%. It is verified the conclusion in Section 4.3 that when a_{xx} = 0.42 ~ 0.65, the surface residual compressive stress in X direction of the workpiece reaches the maximum value. When a_{yy} = 0.36 ~ 0.7, the surface residual compressive stress in Y direction reaches the maximum value.

5. Conclusion

The residual compressive stress has positive significance to improve the service life of thin-walled parts. In this study, a surface residual stress prediction model considering the feed per tooth and the blade edge radius is proposed. The accuracy of the prediction model of surface residual stress and the quantization proportion of the machining parameters of residual compressive stress distribution were verified by experiments. The following conclusions can be drawn:

1. The analysis of milling force and residual stress on workpiece surface shows that the residual stress in X and Y direction on workpiece surface increases with the increase of milling force. The effects of F_x and F_z on the surface residual stress are almost proportional to each other. The milling force increases linearly with the increase of feed per tooth.
2. A surface residual stress prediction model considering milling force-heat and machining parameters was established. Through the analysis of the milling force model, it is found that r and f_z have significant influence on the milling force, and then affects the generation of residual stress on the workpiece surface.
3. Through the analysis of the experimental and simulation results, the quantitative method of machining parameters was proposed combined with the orthogonal milling force model. When $f_z \leq 0.5r$, the maximum residual compressive stress appears on the workpiece surface. When a_{xx}=0.42~0.65, the surface residual compressive stress in X direction reaches the peak value. When a_{yy}=0.36~0.7, the residual compressive stress on the surface in Y direction reaches the peak.

In the future, the influence of milling force variation on residual stress generation of workpiece surface should be further explored. The generation of residual stress in machining can be controlled by further quantitative proportion analysis method of machining parameters. In the following research, other influencing factors of process and tool will be considered comprehensively to establish a more comprehensive quantitative relationship model of machining parameters.

Declarations

Funding information

This paper is supported by National Natural Science Foundation of China (Grant No. 52175427) and Key Project of National Defense Basic Scientific Research (JCKY2020203B037).

Conflict of interest

The authors declare that they have no conflict of interest.

Availability of data and materials

The data and materials that support the findings of this study are available from the corresponding author upon reasonable request.

Ethical Approval

Compliance with ethical standards.

Consent to Participate and Publish

The authors agreed to participate and publish.

Authors' Contributions

Xiaohui Jiang: Conceptualization, Methodology. Yan Cai: Data curation, Validation, Writing- Original draft preparation. Weiqiang Liu: Visualization. Miaoxian Guo: Investigation. Hong Zhou: Writing- Reviewing. Zhou Xu: Editing. Xiangjing Kong: Modeling. Pengfei Ju: Provide experimental cases.

References

1. Jiang, X.H., Kong, X.J., Zhang, Z.Y., Wu, Z.P., Ding, Z.S., Guo, M.X..(2020) Modeling the effects of Undeformed Chip Volume (UCV) on residual stresses during the milling of curved thin-walled parts. International Journal of Mechanical Sciences 167:1-14.
2. Lv, Y.T., Ding, Y., Cui, H.Z., Liu, G.H., Wang, B.H., Cao, L.M., Li, L., Qin, Z.B., Lu, W.J..(2020) Investigation of microscopic residual stress and its effects on stress corrosion behavior of NiAl bronze alloy using in situ neutron diffraction/EBSD/tensile corrosion experiment. Materials Characterization 164:1-12.
3. Chighizola, C.R., D'Elia, C.R., Weber, D., Kirsch, B., Aurich, J.C., Linke, B.S., Hill, M.R. .(2021) Intermethod Comparison and Evaluation of Measured Near Surface Residual Stress in Milled Aluminum. Experimental Mechanics 61(8):1-14.
4. Wu, Q., Xie, D.J., Si, Y., Zhang, Y.D., Zhao, Y.X.. (2018) Simulation analysis and experimental study of milling surface residual stress of Ti-10V-2Fe-3Al. Journal of Manufacturing Processes 32:530-537.
5. Rahul, Y., Vipindas, K., Mathew, J.. (2021) Methodology for prediction of sub-surface residual stress in micro end milling of Ti-6Al-4V alloy. Journal of Manufacturing Processes 62:600-612.
6. Woste, F., Kimm, J., Bergmann, J.A., Theisen, W., Wiederkehr, P.. (2021) Investigation of the effect of residual stresses in the subsurface on process forces for consecutive orthogonal cuts. Production Engineering-Research and Development 15(6):873-883.
7. Jiang, X.H., Zhu, Y.H., Zhang, Z.Y., Guo, M.X., Ding, Z.S.. (2018) Investigation of residual impact stress and its effects on the precision during milling of the thin-walled part. International Journal of Advanced Manufacturing Technology 97(1-4):877-892.
8. Ji, C.H., Sun, S.Q., Lin, B., Fei, J.X.. (2018) Effect of cutting parameters on the residual stress distribution generated by pocket milling of 2219 aluminum alloy. Advances in Mechanical Engineering 10(12):1-15.
9. Clauss, B., Nestler, A., Schubert, A., Dietrich, D., Lampke, T.. (2019) Influencing the Properties of the Generated Surface by Adjusted Rake and Clearance Angles in Side Milling of Aluminum Matrix Composites with MCD-Tipped Tools. Journal of Manufacturing and Materials Processing 3(3):1-20.
10. Borysenko, D., Karpuschewski, B., Welzel, F.,Kundrak, J., Felho, C.. (2019) Influence of cutting ratio and tool macro geometry on process characteristics and workpiece conditions in face milling. Cirp Journal of Manufacturing Science and Technology 24:1-5.
11. Holmberg, J., Wretland, A., Berglund, J., Bene, T.. (2020) A detailed investigation of residual stresses after milling Inconel 718 using typical production parameters for assessment of affected depth. Materials Today Communications 24:1-12.
12. Liang, X.L., Liu, Z.Q., Wang, B., Song, Q.H., Cai, Y.K., Wan, Y.. (2021) Prediction of residual stress with multi-physics model for orthogonal cutting Ti-6Al-4V under various tool wear morphologies. Journal of Materials Processing Technology 288:1-12.
13. Liu, Y., Xu, D.D., Agmell, M., Rachid, M., Aylin, A., Stahl, J., Zhou, J.M.. (2021) Numerical and experimental investigation of tool geometry effect on residual stresses in orthogonal machining of Inconel 718. Simulation Modelling Practice and Theory 106:1-15.
14. Yi, S.H., Wu, Y.X., Gong, H., Peng, C.X., He, Y.B.. (2021) Experimental Analysis and Prediction Model of Milling-Induced Residual Stress of Aeronautical Aluminum Alloys. Applied Sciences-Basel 11(13):1-15.
15. Cheng, M.H., Jiao, L., Yan, P., Feng, L.C., Qiu, T.Y., Wang, X.B., Zhang, B.R.. (2021) Prediction of surface residual stress in end milling with Gaussian process regression. Measurement 178:1-11.
16. Zhou, R.H., Yang, W.Y.. (2019) Analytical modeling of machining-induced residual stresses in milling of complex surface. International Journal of Advanced Manufacturing Technology 105(1-4):565-577.
17. Wolfle, C.H., Wimmer, M., Hameed, M.Z.S., Christian, K., Michael, Z., Ewald, W.. (2020) Towards real-time prediction of residual stresses induced by peripheral milling of Ti-6Al-4V. Continuum Mechanics and Thermodynamics 33:1023-1039.
18. Yue, C.X., Hao, X.L., Ji, X., Liu, X.L., Liang, S.Y., Wang, L.H., Yan, F.G.. (2020) Analytical Prediction of Residual Stress in the Machined Surface during Milling. Metals 10(4):1-20.
19. Yang, S.C., Ren, W., Wang, T.J., Su, S.. (2020) Parameter optimization of a micro-textured ball-end milling cutter with blunt round edge. International Journal of Advanced Manufacturing Technology 106(5):577-588.
20. Ma, Y., Ding, W.Y., Ping, F.F.. (2014) FEM Analysis of Residual Stress Distribution and Cutting Forces in Orthogonal Cutting with Different Initial Stresses. Materials Science Forum 3256(800-801):380-384.

21. Zhou, Y.D., Tian, Y.L., Jing, X.B., Kornel, F.E.. (2017) A novel instantaneous uncut chip thickness model for mechanistic cutting force model in micro-end-milling. International Journal of Advanced Manufacturing Technology 93(5-8):2305-2319.
22. Srinivasa, Y.V., Shunmugam, M.S.. (2013) Mechanistic model for prediction of cutting forces in micro end-milling and experimental comparison. International Journal of Machine Tools & Manufacture 67:18-27.
23. Wyen, C.F., Wegener, K.. (2010) Influence of cutting edge radius on cutting forces in machining titanium. Cirp Annals-Manufacturing Technology 59(1):93-96.
24. Jiang, X.H., Kong, X.J., He, S.R., Wu, K.. (2021) Modeling the superposition of residual stresses induced by cutting force and heat during the milling of thin-walled parts. Journal of Manufacturing Processes 68:356-370.
25. Ma, Y., Feng, P.F., Zhang, J.F.,Wu, Z.J.,Yu, D.W.. (2016) Prediction of surface residual stress after end milling based on cutting force and temperature. Journal of Materials Processing Technology 235:41-48.
26. Lin, Y.C., Jiang, Y.Q., Zhou, H.M.,Liu, G.. (2014) A New Creep Constitutive Model for 7075 Aluminum Alloy Under Elevated Temperatures. Journal of Materials Engineering and Performance 23(12):4350-4357.
27. Tzotzis, A., Garcia, H.C., Huertas, T.J.L., Kyratsis, P.. (2020) FEM based mathematical modelling of thrust force during drilling of Al7075-T6. Mechanics & Industry 21(4):1-14.
28. Li, B.Z., Jiang, X.H., Jing, H.J., Zuo, X.Y.. (2011) High-speed milling characteristics and the residual stresses control methods analysis of thin-walled parts.In Modelling of Machining Operations 1243(223):456-471

Figures

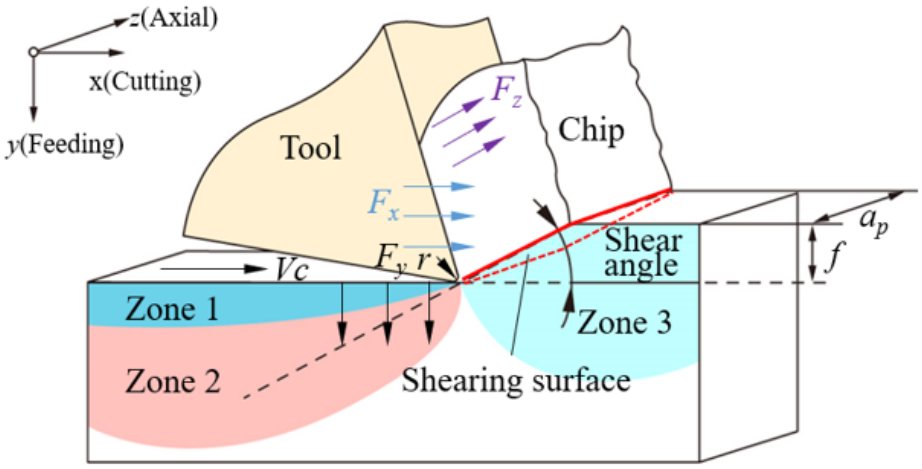

Figure 1

Orthogonal model of cutting load and stress zone

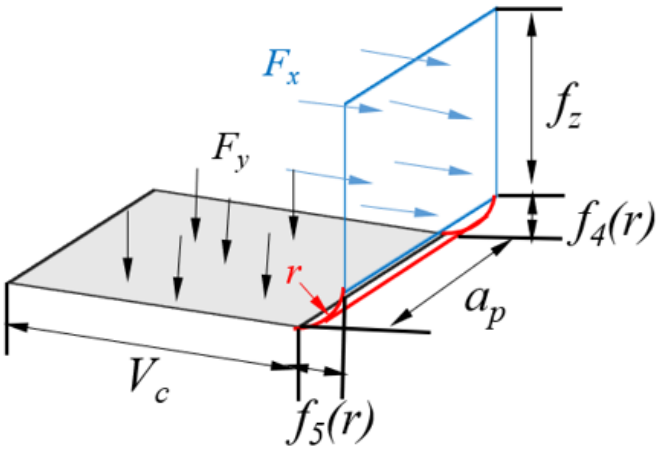

Figure 2

Assumed cutting force equivalent projection plane

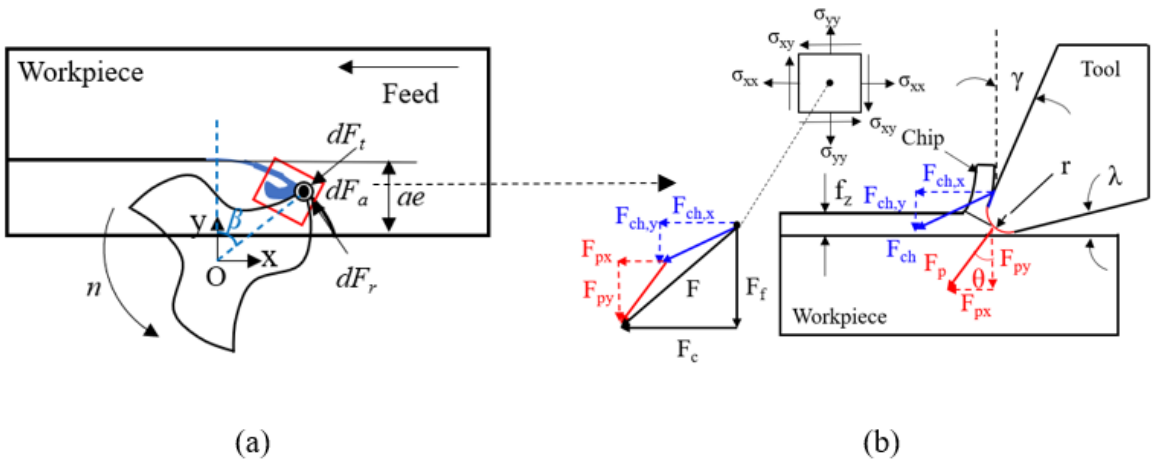

Figure 3

The milling force model of the workpiece

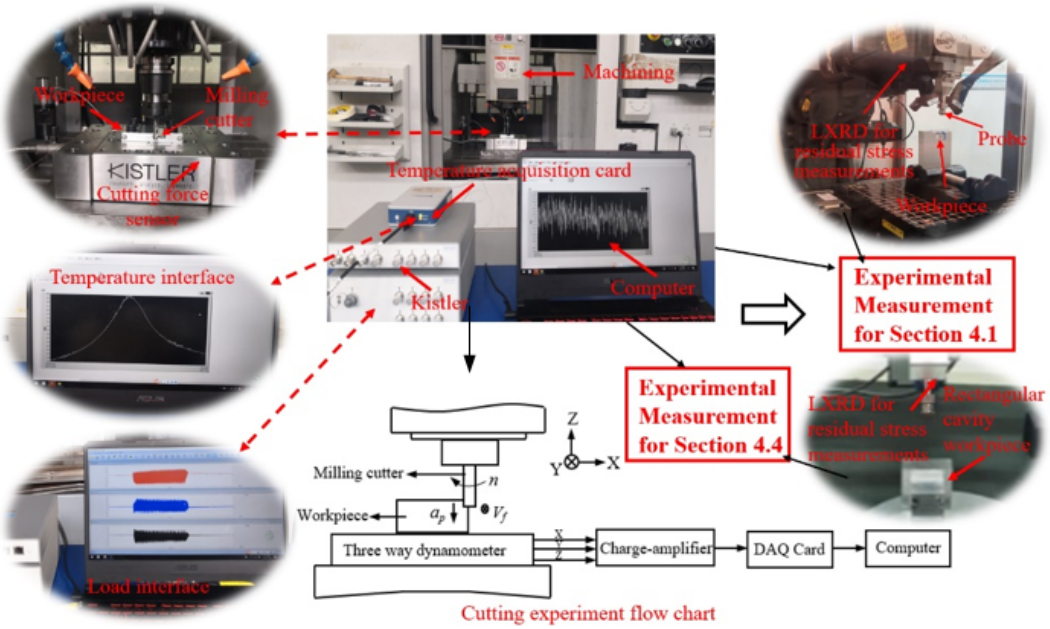

Figure 4

Experimental processing and measurement process

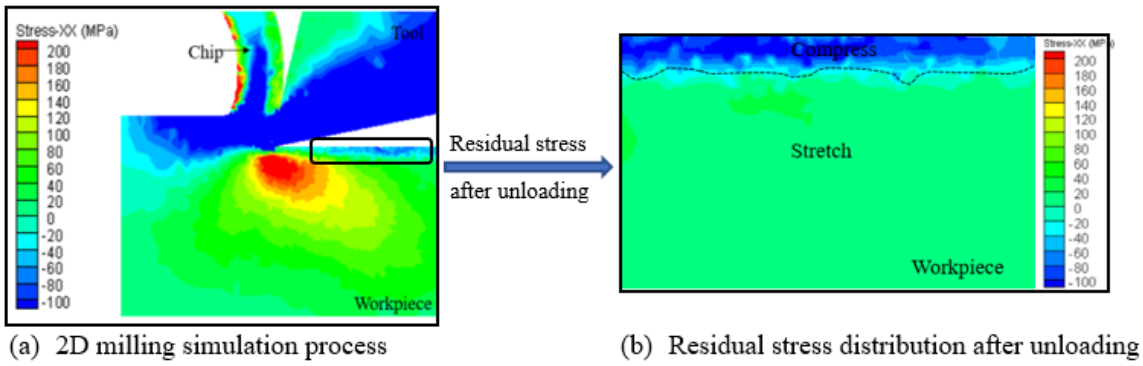

(a) 2D milling simulation process (b) Residual stress distribution after unloading

Figure 5

Simulation results of orthogonal cutting

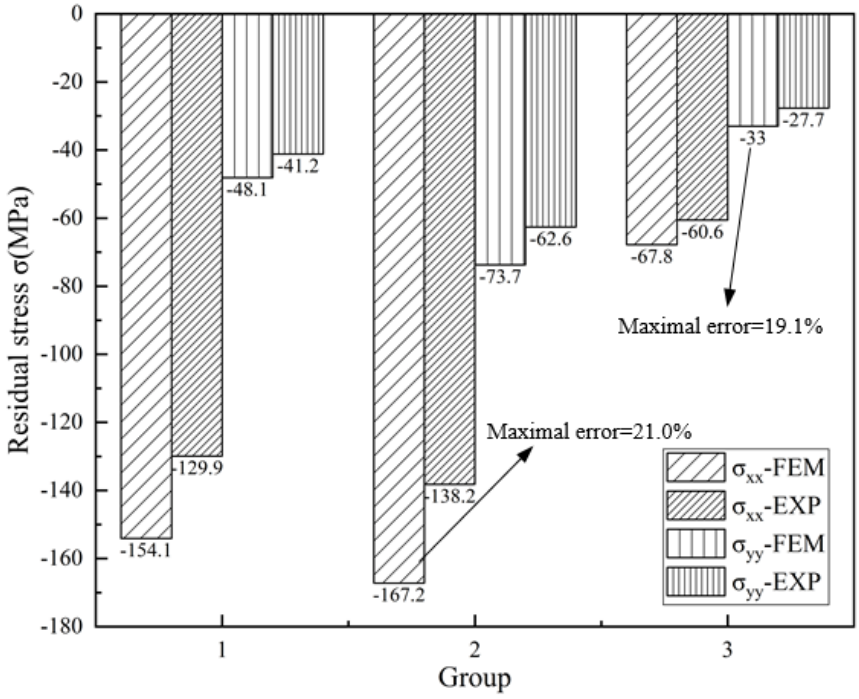

Figure 6

Simulation and experimental comparison of surface residual stress

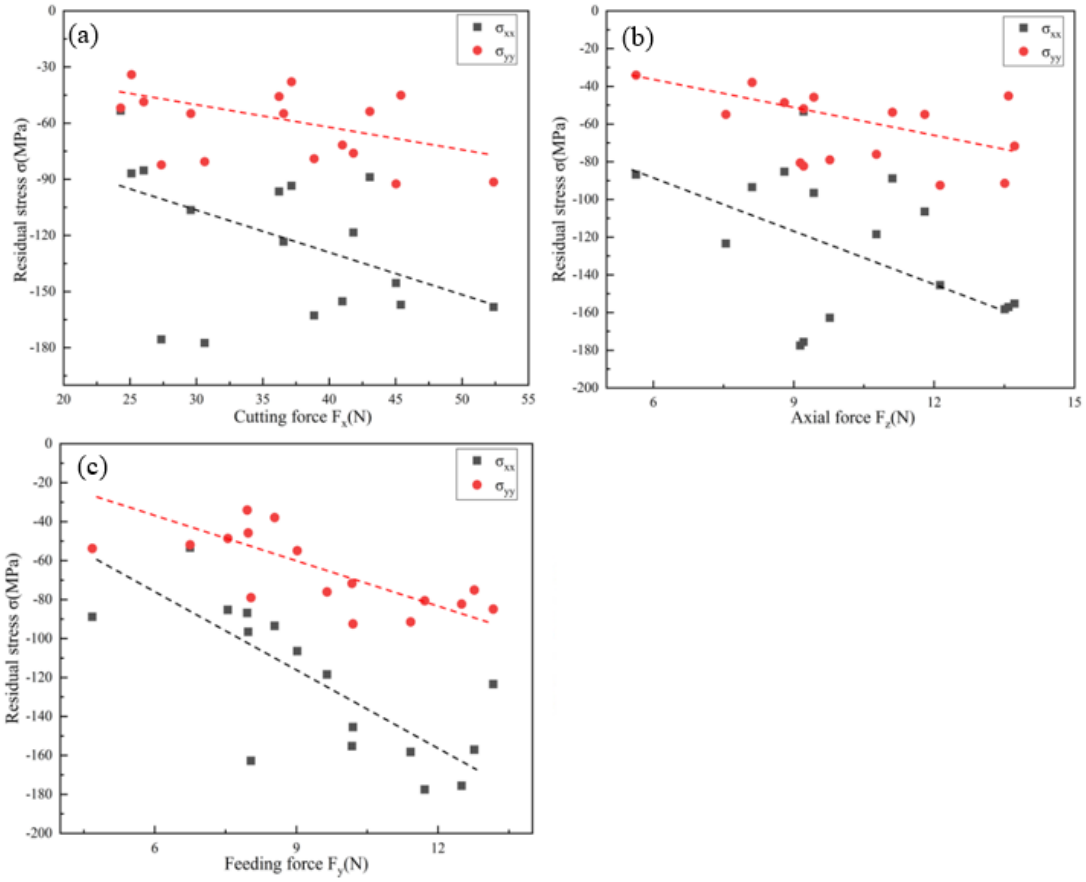

Figure 7

(a)-(c) is the relationship between milling forces

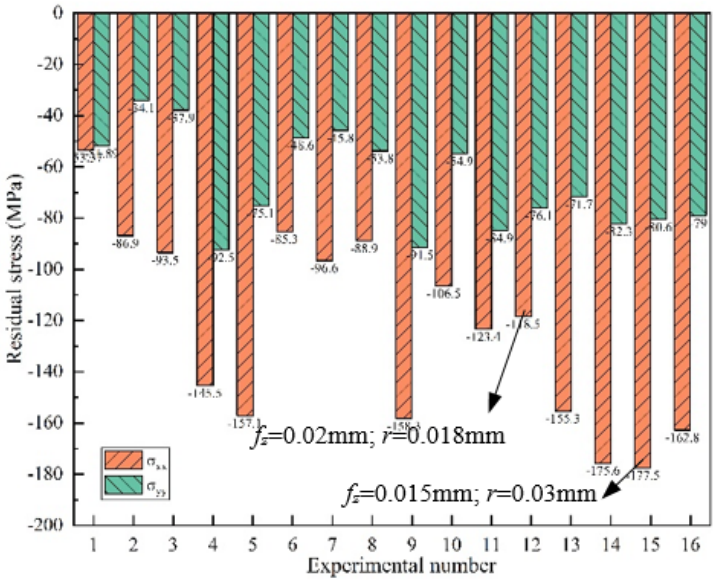

Figure 8

Residual stress on workpiece surface

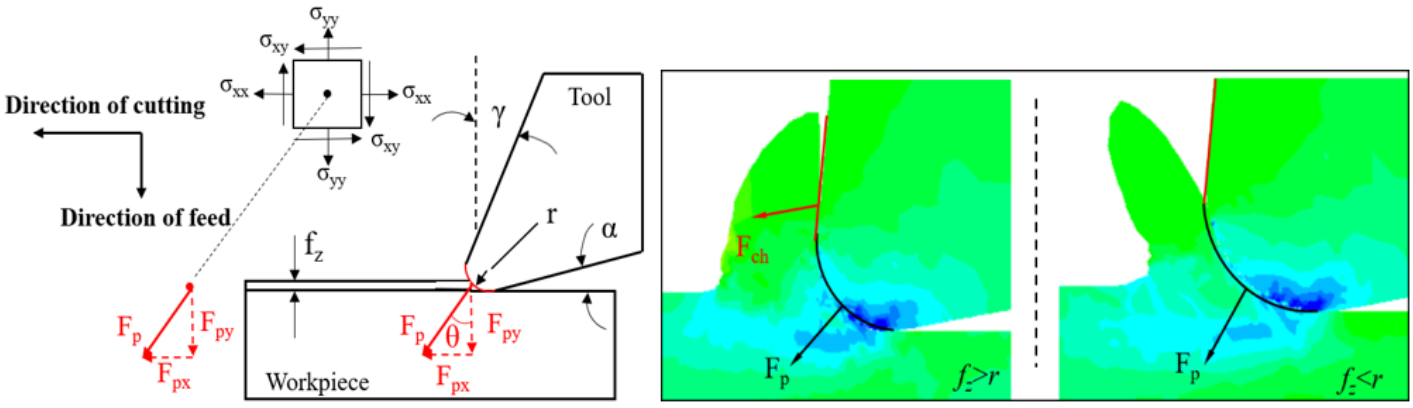

(a) Schematic diagram of two-dimensional orthogonal milling

(b) Force diagram of milling simulation

Figure 9

The stress condition of a milling workpiece

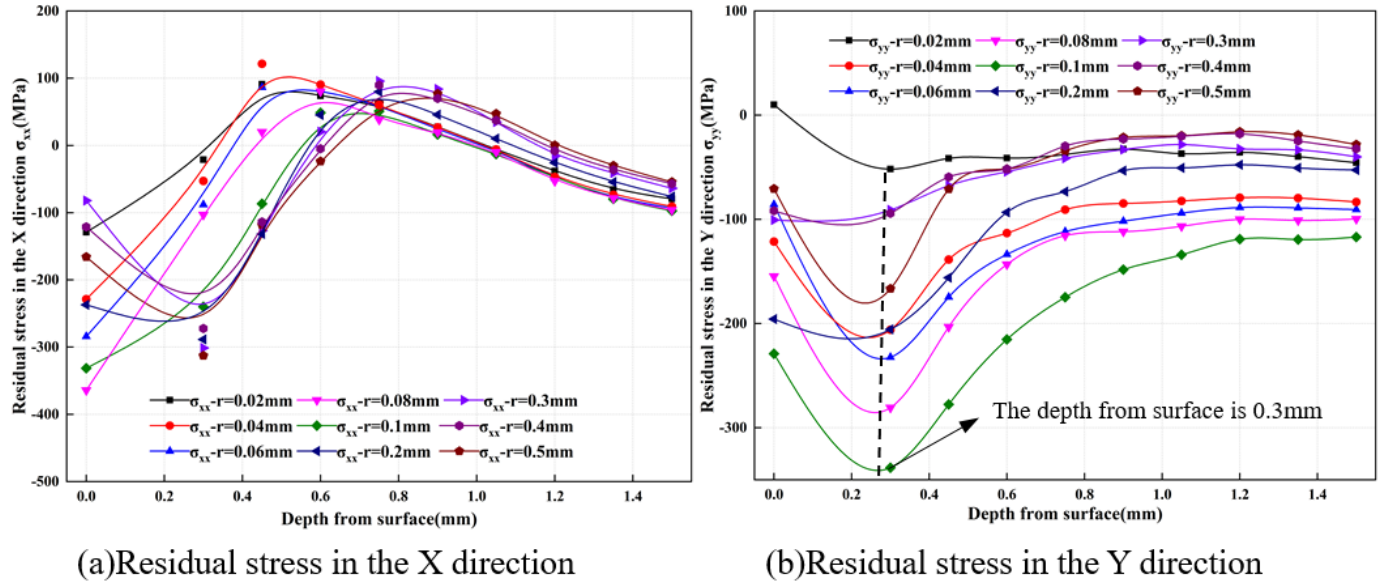

(a)Residual stress in the X direction (b)Residual stress in the Y direction

Figure 10

Residual stress curve corresponding to different blade edge radius

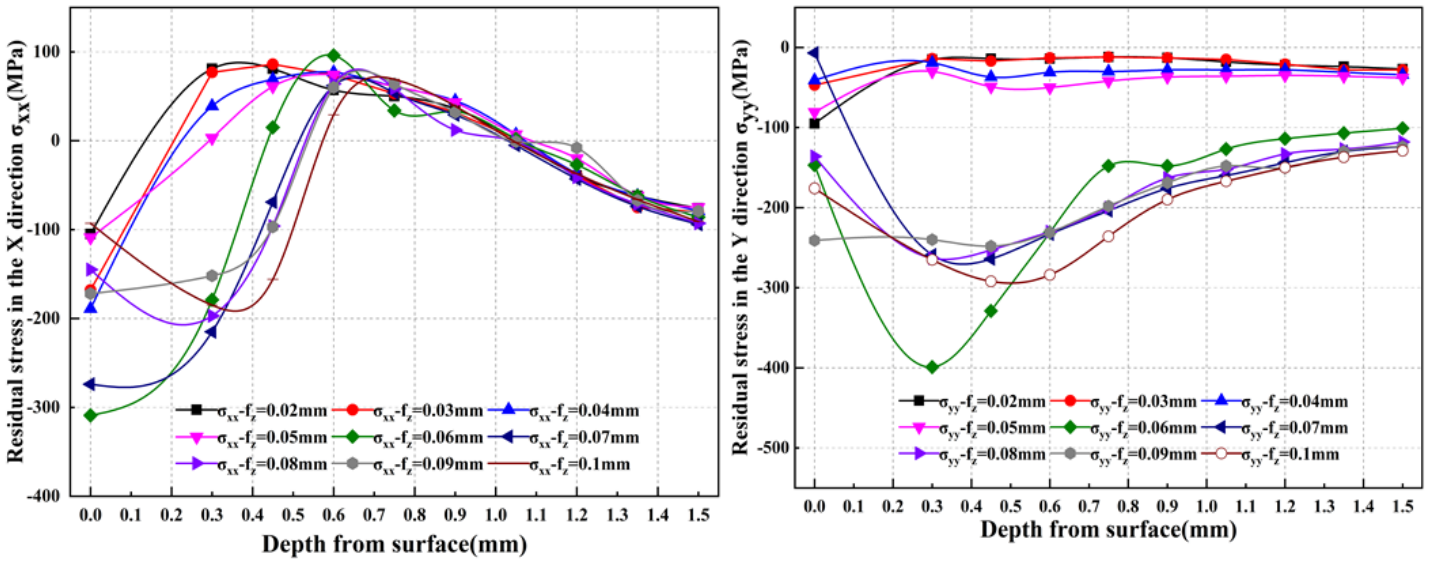

(a) Residual stress in the X direction (b) Residual stress in the Y direction

Figure 11

Influence of different f_z on residual stress（r=0.1mm）

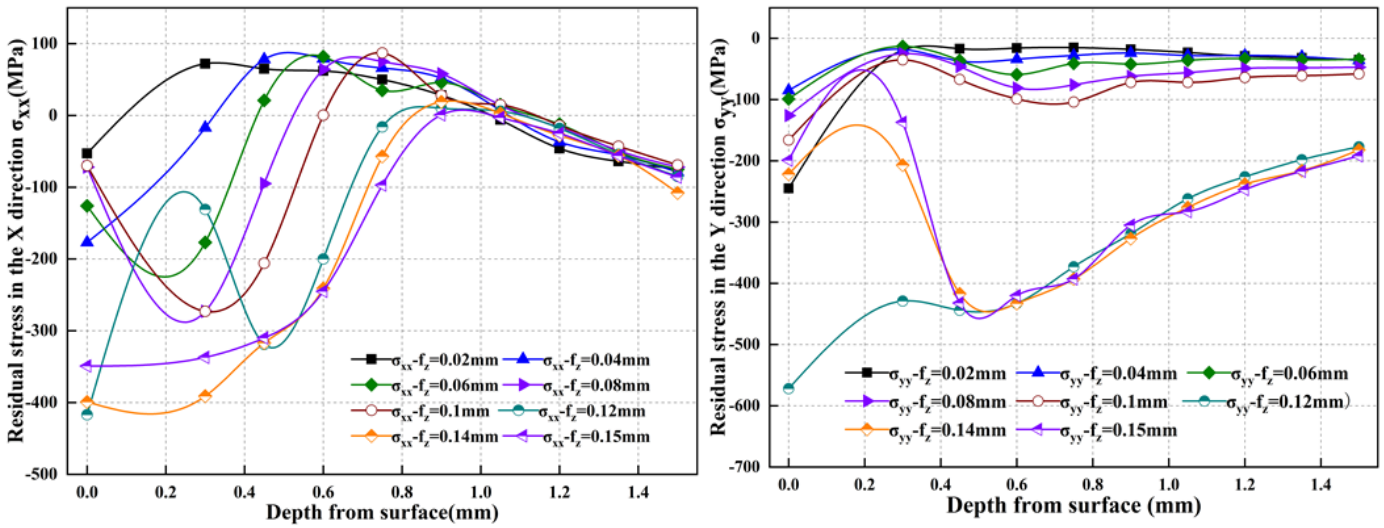

(a)Residual stress in the X direction (b)Residual stress in the Y direction

Figure 12

Influence of different f_z on residual stress（r=0.2mm）

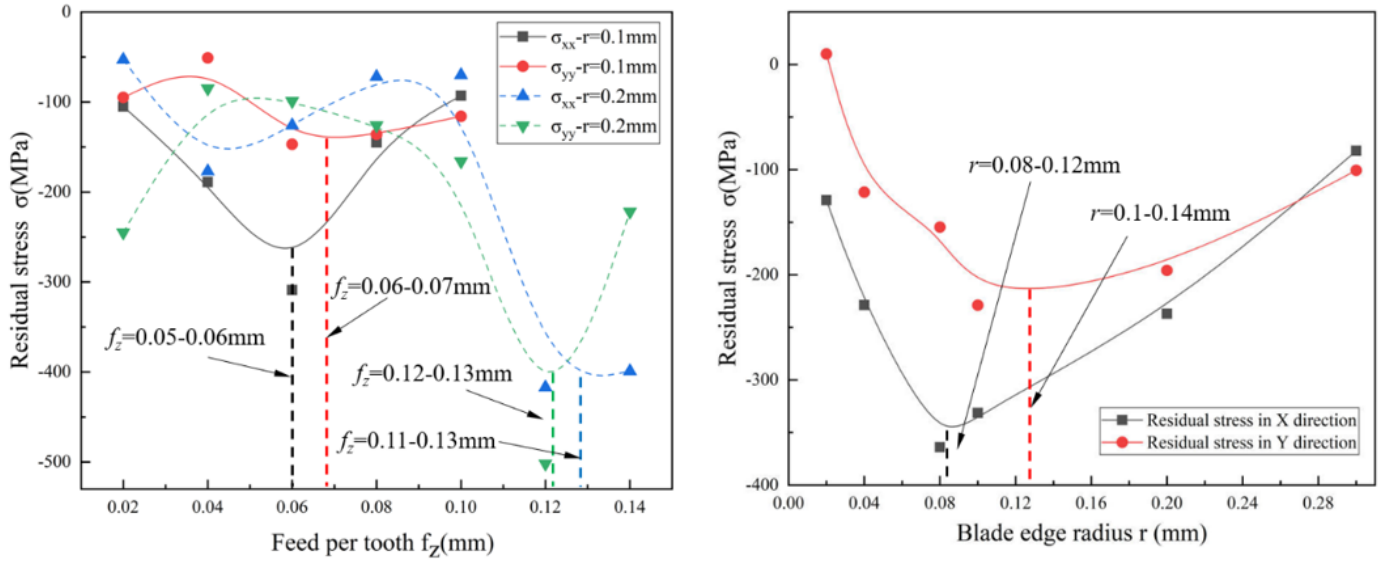

(a) The variation trend of residual stress with f_z (b) The variation trend of residual stress with r

Figure 13

Residual stress distribution on workpiece surface

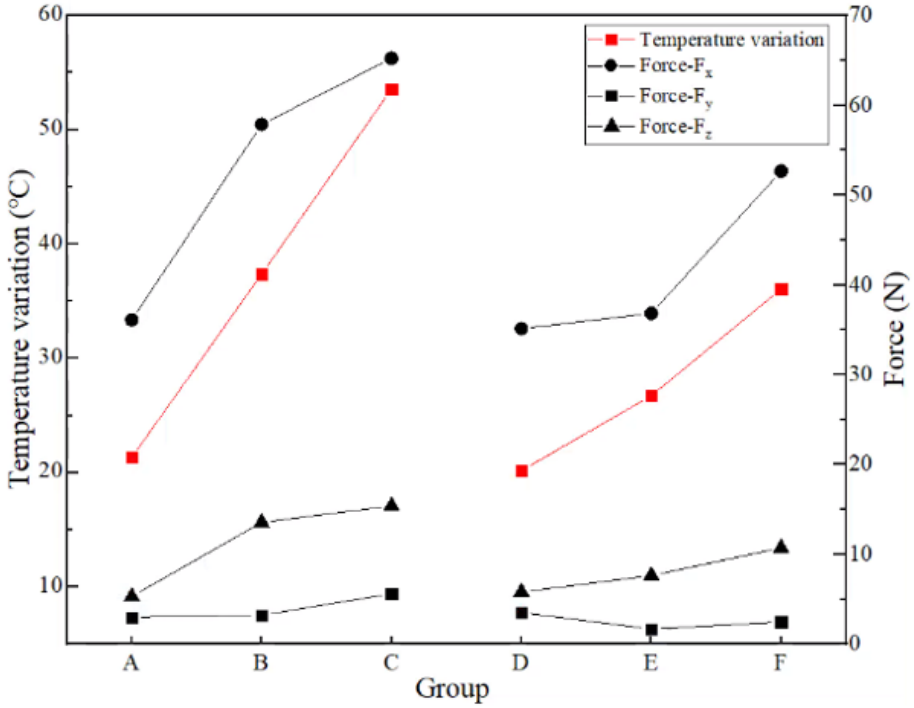

Figure 14

Force and temperature measurements

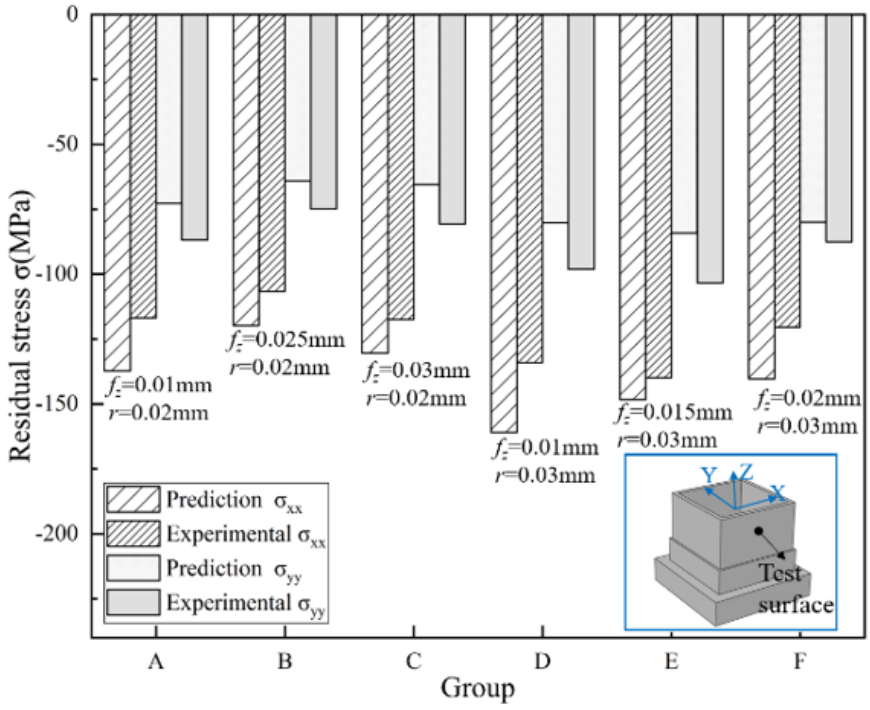

Figure 15

Calculated and measured residual stress